# 1 Impact of stratospheric intrusion on near-surface ozone over

# 2 the Sichuan Basin in China driven by terrain forcing of

# 3 Tibetan Plateau

13

14

15

16

17

18

19

20

21

22

23

24

25

26

27

28

29

30

31

- Zhuozhi Shu<sup>a,b</sup>, Fumo Yang<sup>c</sup>, Guangming Shi<sup>c</sup>, Yuqing Zhang<sup>b</sup>, Yongjie Huang<sup>a</sup>, Xinning Yu<sup>a</sup>,
  Baiwan Pan<sup>a</sup>, Tianliang Zhao<sup>b\*</sup>
- 6 a Chengdu Fluid Dynamics Innovation Center, Chengdu 610031, China
- 7 b Key Laboratory for Aerosol-Cloud-Precipitation of China Meteorological Administration,
- 8 Collaborative Innovation Center on Forecast and Evaluation of Meteorological Disasters,
- 9 Nanjing University of Information Science and Technology, Nanjing Jiangsu 210044, China
- <sup>c</sup> School of Carbon Neutrality Future Technology, National Engineering Research Center on
- 11 Flue Gas Desulfurization, Sichuan University, Chengdu, 610065, China
- 12 Correspondence: Tianliang Zhao (tlzhao@nuist.edu.cn)

Abstract. Stratospheric ozone (O<sub>3</sub>) intrusion acts as a major natural source of tropospheric O<sub>3</sub> affecting atmospheric environment. Targeting a stratospheric intrusion (SI) hotspot, the Tibetan Plateau (TP) with the immediately adjoining O<sub>3</sub> pollution region of Sichuan Basin (SCB) in Southwest China, this study assesses the seasonal contribution of SI to the near-surface O<sub>3</sub> over SCB and reveals the multi-scale coupling mechanisms of atmospheric circulations with the seasonally discrepant terrain effects of the TP. Based on the simulations on four selected SI events in 2017, it is estimated that SI over the TP can penetrate deeply into the near-surface atmosphere in SCB, with event-specific maxima of up to 38.7% in O<sub>3</sub> increments, providing an extra contribution of 11.1–16.0% to regional O<sub>3</sub> pollution. The evolution of South Asian High with the peripheral subsidence in the warm seasons and the subtropical jet structure in the cold seasons facilitates tropopause folding, driving stratospheric O<sub>3</sub> into the free troposphere. We further identified the dominant processes for SI-derived O<sub>3</sub> entering the near-surface layer over the basin with 1) a direct intrusion pathway of downward transport over the central and eastern SCB regions in the warm seasons, and 2) an indirect pathway of downslope transport along the TP-SCB slope into the western SCB region in the cold season, revealing the distinct seasonal effects of TP thermal and mechanical forcing on stratospheric O<sub>3</sub> transport into the SCB region. These findings highlight the critical role of the TP in modulating stratosphere-to-troposphere O<sub>3</sub> transport and its implications for regional air quality changes.

- **Key words:** Stratospheric ozone intrusion; Tibetan Plateau's terrain forcing; multi-scale
- 34 atmospheric circulations; seasonality; Sichuan Basin.

### 1 Introduction

35

36

37

38

39

40

41

42

43

44

45

46

47

48

49

50

51

52

53

54

55

56

57

58

59

60

61

62

63

Ozone (O<sub>3</sub>) is a crucial atmospheric chemical composition. Stratospheric ozone (accounting for approximately 90% of the O<sub>3</sub> column) can absorb harmful ultraviolet radiation and protect the surface biosphere, while tropospheric O<sub>3</sub> has emerged as one of the most important air pollutants due to its direct impact on climate change, ecosystem, atmospheric oxidation and human health (Fiore et al., 2002; Feng et al., 2015; Miri et al., 2016). Tropospheric O<sub>3</sub> mainly originates from photochemical production and stratospheric intrusion. The former is characterized by complex nonlinear reactions of O<sub>3</sub> precursors from anthropogenic and natural emissions, involving carbon monoxide, volatile organic compounds and nitrogen oxides, etc. In comparison, the downward transport of stratospheric O<sub>3</sub> not only provides an additional natural source for tropospheric O<sub>3</sub> budgets but causes uncertainties in the near-surface atmospheric environmental changes (Lin et al., 2012; Monk et al., 2015; Liu et al., 2022). Stratospheric intrusion (SI) is an atmospheric dynamic process occurring between the lower stratosphere and upper troposphere, characterized by the cross-tropopause transport of stratospheric dry airflows into troposphere with rich O<sub>3</sub> and high-level potential vorticity. Multiscale atmospheric physical processes can trigger SI, including Brewer-Dobson circulation (Brewer, 1949; Dobson et al., 1956; Burchart, 2014), Rossby wave breaking, ENSO, subtropical jet stream, cut-off low, mesoscale convection, and tropopause folding (Waugh and Polvani, 2000; Sprenger et al., 2003; Nieto et al., 2005; Koumoutsaris et al., 2008; Trickl et al., 2011; Neu et al., 2014; Venkat et al., 2016). Approximately  $540 \pm 140 \text{ Tg yr}^{-1}$  stratospheric O<sub>3</sub> enters the troposphere through SI worldwide, contributing ~30% of the tropospheric O<sub>3</sub> column (Stohl et al., 2003; Young et al., 2013). Global SI distribution exhibits a distinct zonal and seasonal asymmetry where the SI hotspots are located in the subtropical regions during late winter and early spring (Škerlak et al., 2014; Williams et al., 2019). The peak of tropopause folding frequency in the period even induces deep SI affecting the lower troposphere (Trickl et al., 2014; Zhao et al., 2021; Chen et al., 2023) which leads to the "exceptional events" on air quality changes (Lin et al., 2015; Pierce and Holloway, 2017). Therefore, cross-layer transport of stratospheric O<sub>3</sub> has a non-negligible potential impact on the near-surface ambient atmosphere, especially over the susceptive regions of SI (e.g. the west coast of North America, Northwest coast of Africa, eastern Mediterranean and Tibetan Plateau) (Škerlak et al., 2015; Lee et al., 2024).

Tibetan Plateau (TP) is the highest plateau referred as "the roof of the world", located in the mid-latitude region over the Eurasian continent. Large-topography forcing not only modulates hemispheric-scale atmospheric circulation patterns but forms a key window of mass exchange between stratosphere and troposphere (Fu et al., 2006; Li et al., 2018; Huang et al., 2023). As a global hotspot for SI (Škerlak et al., 2014), the impacts of SI on tropospheric O<sub>3</sub> over TP have been extensively studied in recent years. Previous results pointed out that the subtropical jet stream is the principal driving factor for frequent SI events over the TP (Zhang et al., 2010; Luo et al., 2019), dominating the vertical distribution of tropospheric O<sub>3</sub> (Yang et al., 2022; Yin et al., 2023). The O<sub>3</sub>-rich airflows from SI can subsequently extend downward to the deep planetary boundary layer by intense turbulent mixing (Chen et al., 2011; Chou et al., 2023), remarkably affecting seasonal and diurnal variations of near-surface O<sub>3</sub> in the region (Ding and Wang, 2006; Ma et al., 2014; Yin et al., 2017). However, with the distinct topography of TP and frequent SI occurrence, few studies consider the impacts of residual O3-rich from SI on atmospheric environmental changes over downstream regions of westerlies, particularly in the typical pollution regions. Addressing this gap, further exploring the impacts of cross-layer O<sub>3</sub> transport from the free troposphere on atmospheric environmental changes in the flat region under the mid-latitude prevailing westerlies is of great value.

Sichuan Basin (SCB), located immediately adjacent to the eastern TP, is recognized as a key region of air pollution complex in China (Lu et al., 2018; Wang et al., 2022) with persistently elevated near-surface O<sub>3</sub> levels (Wei et al., 2022). Regarding the frequent O<sub>3</sub> pollution in SCB, extensive research focuses on the meteorology-emission synergy effects on atmospheric environmental variability, including photochemical regime (Kong et al., 2023), horizontal transport and residual layer mixing (Shu et al., 2023; Wang et al., 2023) and biological source contribution (Xian et al., 2024). Notably, subsidence momentum in the middle and lower free troposphere coexists with the forced uplift of the East Asian monsoon over SCB, ascribed to mechanical forcing of TP's terrain on prevailing airflows (Xu et al., 2016; Shu et

al., 2022), which significantly enhance the vertical interactions of atmospheric pollutants between the free troposphere and atmospheric boundary layer (Shu et al., 2021; Hu et al., 2023). Such regional vertical circulation patterns create excellent atmospheric dynamical conditions for SI to affect the <u>ambient atmosphere</u> over SCB. Therefore, investigating the multi-scale atmospheric circulation coupling mechanisms for stratospheric O<sub>3</sub> into the ambient atmosphere under the plateau-basin topography can provide critical insights into understanding the uncertainty of O<sub>3</sub> pollution in China.

In this study, we aim to quantify the contribution of SI to near-surface  $O_3$  levels over the SCB and then to elucidate the multi-scale circulation coupling mechanisms, in particular focusing on their seasonality with the thermodynamic and dynamical forcing of TP and SCB. The findings of our study are expected to improve the understanding of atmospheric environmental effects of the TP with implications for global and regional environmental changes. Section 2 introduces the observational and reanalysis data, SI episodes selection, WRF-Chem model configuration, experiments design and modeling evaluation results. Section 3 analyzes the temporospatial variations of SIs' impacts on the near-surface layer over the SCB and the terrain-induced atmospheric circulation mechanisms on cross-layer transport of  $O_3$  from stratosphere into the atmospheric boundary layer. Finally, the conclusion are provided in Sect. 4.

### 2 Data and method

### 2.1 Observational and reanalysis data

The hourly ground-based observations of environment and meteorology (near-surface O<sub>3</sub> concentrations, 2 m air temperature (T2), 10 m wind speed (WS10) and near-surface relative humidity (RH)) in the study region are respectively obtained from the China National Environmental Monitoring Center (<a href="http://www.cnemc.cn/">http://www.cnemc.cn/</a>) and the Chinese Meteorological Monitoring Network (<a href="http://data.cma.cn/">http://data.cma.cn/</a>) to evaluate WRF-Chem model performance during the SI episodes.

The hourly 3D meteorological reanalysis data ERA5, with a horizontal resolution of 0.25°×0.25°, are derived from the European Center for Medium-Range Weather Forecasts

(https://cds.climate.copernicus.eu/datasets). In the study, this dataset is not only used for SI identification and atmospheric circulation evolution analysis but also serves as the initial and boundary conditions of WRF-Chem experiments. Additionally, the Copernicus Atmosphere Monitoring Service (CAMS) global atmospheric composition reanalysis dataset EAC4 (https://ads.atmosphere.copernicus.eu/datasets) provides 3-hourly chemical species data with a horizontal resolution of 0.75°×0.75° and 60 vertical layers, presenting great credibility in the environment-chemistry field (Inness et al., 2019). The stratospheric O<sub>3</sub> tracer (O<sub>3</sub>S) from EAC4 is utilized to verify WRF-Chem simulation applicability for quantifying the transport contributions of SI.

### 2.2 Selection of seasonal SI episodes

The months of April, July, October and January in the year 2017 are chosen to characterize seasonal variations in SI and atmospheric circulation patterns in the study as a sequel to our previous studies (Shu et al., 2022; Shu et al., 2023). Corresponding pressure-time cross sections of O<sub>3</sub> averaged over the regions of eastern TP (90-100°E, 28-33°N) and SCB (103-110°E, 28-33°N) are shown in Fig. 1. It is found that frequent stratospheric O<sub>3</sub> intrusions appear over the eastern TP region and significantly affects the middle troposphere with deep SI during April and January but shallow SI in the months of July and October, which is consistent with SI seasonality in the previous results (Škerlak et al., 2014; Luo et al., 2019). With the middlelatitude westerlies transport, the O<sub>3</sub>-rich air from SI is stretched and deepens into the lower troposphere (reaching 700 hPa layer) over the SCB. In this study, four SI events were selected based on vertical O<sub>3</sub> structures over the eastern TP and SCB, prioritizing peak SI intensity and significant impacts on the lower-tropospheric O<sub>3</sub> concentrations. The strongest-impact cases within their respective months occurring during 12-17 April (EP1), 1-3 July (EP2), 23-28 October (EP3), and 26–30 January (EP4) (Fig. 1) serve as typical seasonal representatives. Their selection enables clear elucidation of seasonal atmospheric circulation mechanisms and quantitative O<sub>3</sub> contributions to near-surface pollution.

Tropopause folding frequently occurs in the TP characterized by perturbance in dynamical tropopause (2 PVU, potential vorticity unit) isosurface associated with downward cross-tropopause exchange (Sprenger et al., 2003; Luo et al., 2019). As shown in Fig. 2, there exist

tropopause folding phenomena that induce O<sub>3</sub>-rich stratospheric airflows injecting into the free troposphere between 28–34°N in the study period. Notably, the intensity and location of SIs are influenced by the distinct seasonality of vertical motion in the atmosphere. While alternating rising and sinking momentum leads to a deep SI event over the central TP during EP1, the deep convection of TP in EP2 triggers strong stratospheric O<sub>3</sub> transport into the lower troposphere (exceeding 160 ppb at 700 hPa layer) over the TP's downstream region SCB. By comparison, a similar vertical structure of SIs in both EP3 and EP4 is featured with the shallow tropopause folding which happens above 300 hPa with weak downward transport of stratospheric O<sub>3</sub>.



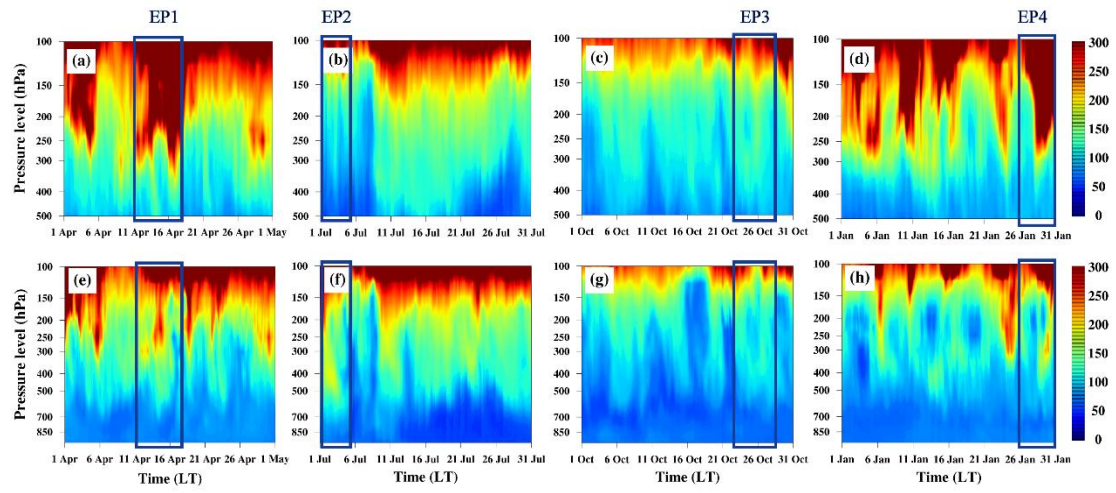


Fig 1. Vertical-time cross sections of O<sub>3</sub> mixing ratio (ppb) over the TP (upper panels) and SCB (lower panels) during April (a,e), July (b,f), October (c,g) and January (d,h) in 2017. The dark-blue boxes respectively represent the selected four SI episodes (EP1–EP4).

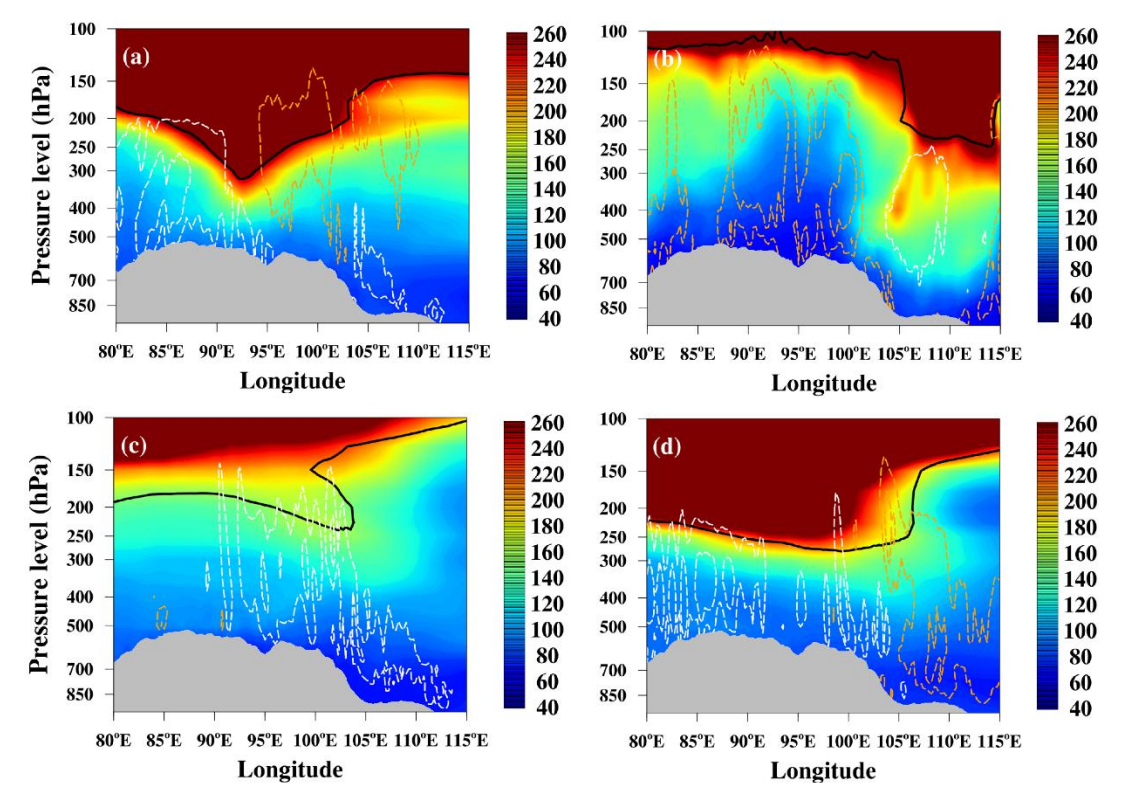


Fig 2. Height-longitude cross sections of  $O_3$  mixing ratio (ppb) averaged between 28–34 °N on (a) 15 April, (b) 1 July, (c) 26 October and (d) 28 January in 2017. The black lines indicate tropopause heights (2 PVU) with the updrafts (brown dashed lines) and downdrafts (white dashed lines) in the region.

# 2.3 Model configuration and experimental design

The fully online weather-chemistry coupled model WRF-Chem (version 3.8.1) is employed to simulate the variations of meteorology and O<sub>3</sub> for this study. Three nesting domains are constructed (shown in Fig. S1) with horizontal model grid intervals respectively of 48 km, 12 km and 3 km and 40 vertical levels from the surface layer to model top at 50 hPa. The ERA5 reanalysis data are served as the meteorological initial and boundary conditions for WRF-Chem simulation. The first 3 days of simulation are the spin-up time to fully depict SI processes driven by atmospheric circulations. The main physical and chemical schemes are listed in Table S1. Anthropogenic air pollutant emissions are obtained from the Multi-resolution Emission Inventory for China (MEIC, 2017) with a horizontal resolution of 0.25°×0.25° (http://www.meicmodel.org/). And the Model of Emissions of Gases and Aerosols from Nature (MEGAN, v2.1, Guenther et al., 2012) is applied for biogenic emission in WRF-Chem simulation.

The Upper Boundary Condition (UBC) developed by Barth et al. (2012) is incorporated to revise the values of stratospheric atmospheric chemical species ranging from tropopause to 50 hPa due to the lack of stratospheric chemistry in WRF-Chem model. The key chemical species (ie., CH<sub>4</sub>, CO, O<sub>3</sub>, NO, NO<sub>2</sub>, HNO<sub>3</sub>, N<sub>2</sub>O<sub>5</sub> and N<sub>2</sub>O) are fixed to climatological values from global chemistry model results while the tropopause height is calculated by WACCM results (Barth et al., 2012; Lamarque et al., 2012). Zhao et al. (2021) have proved that WRF-Chem can accurately capture the O<sub>3</sub> transport of SI by utilizing UBC scheme. In addition, the integrated process rate (IPR) analysis is used to deepen the understanding of cross-layer O<sub>3</sub> transport mechanism between the free troposphere and atmospheric boundary layer.

Four groups of simulation experiments are conducted to investigate the impact of SI on atmospheric environmental changes over SCB and related plateau-basin terrain forcing effects as follows: 1) Base experiment (Base), utilize UBC scheme to reproduce 3D meteorology and chemistry during the SI episodes; 2) stratospheric O<sub>3</sub> sensitivity experiment (EXP<sub>stro3</sub>), other settings are identical to Base but discard UBC scheme and default O<sub>3</sub> values (set as zero) above tropopause in WRF-Chem simulation; 3) the basin-terrain sensitivity experiment (EXP<sub>terr</sub>), basin-filling terrain replace the default deep-basin terrain height (take Base as a benchmark), which refers to a zonal linear interpolation method (Zhang et al., 2019), but remain surface static fields (e.g. landuse and soil types) unchanged; 4) both stratospheric O<sub>3</sub> and basin-terrain sensitivity experiment (EXP<sub>stro3+terr</sub>), run with basin-filling terrain compared with EXP<sub>stro3</sub>. To elaborately quantify the contribution of SI in the study, we calculate the relative contributions derived as RC =  $(\Delta x / Base) \times 100\%$ , where  $\Delta x$  is the simulation differences between Base and EXPstro3 experiments ( $\Delta x = Base - EXPstro3$ ), and Base is the Base experiment simulations for O<sub>3</sub> concentrations, horizontal transport (ADVH) and vertical transport (ADVZ). The △O<sub>3</sub>basin = EXP<sub>terr</sub> - EXP<sub>stro3+terr</sub> is used to investigate the deep-basin terrain forcing mechanism on cross-layer transport of O<sub>3</sub> during the SI episodes.

### 2.4 Modeling evaluation

182

183

184

185

186

187

188

189

190

191

192

193

194

195

196

197

198

199

200

201

202

203

204

205

206

207

208

209

210

Our model results can reasonably reproduce the variations in meteorology both at the nearsurface layer and within atmospheric boundary layer by comparing simulated and observed results during the four representative months of April, July, October and January in 2017 (Shu et al., 2023). The statistical metrics of T2, WS10 and RH are also listed in Table S2, which meets the model criteria for applications recommended by Emery et al. (2001).

Regarding the accuracy of simulated surface O<sub>3</sub> concentrations, WRF-Chem simulation results also show a good agreement with ground-based environmental observation at 18 urban sites in the SCB (Shu et al., 2023). Fig. S2 shows the comparisons of near-surface O<sub>3</sub> variations between simulation and observation at two representative megacities of Chengdu and Chongqing during the SI episodes, respectively with the index of agreement (IOA) of 0.68–0.91 (Chengdu) and 0.56–0.89 (Chongqing) and mean fractional error (MFE) ranged of 10.8–20.8% and 18.9–29.7%. Whereafter, the spatial distribution of near-surface ΔO<sub>3</sub> is compared with O<sub>3</sub>S of EAC4 reanalysis data. As shown in Fig. 3, though there exists an overestimation in EP4, the modeling results properly present the impacts of SI on near-surface O<sub>3</sub> levels in our study region. Overall, the evaluation results above present good modeling reliability for the following analyses (Fig. S3).

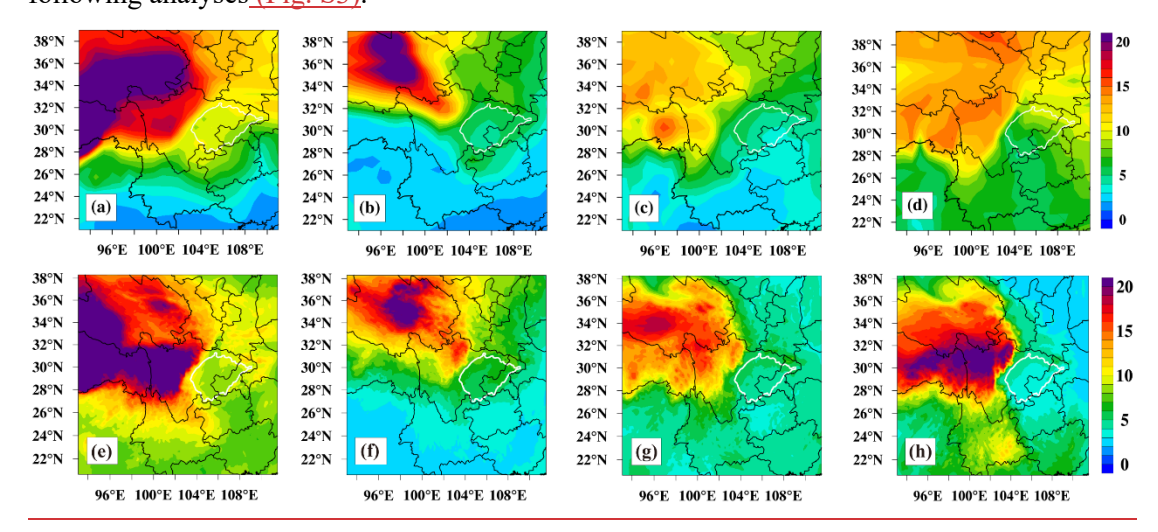


Fig 3. Comparisons of near-surface layer  $\triangle O_3$  (ppb) between EAC4 (upper panels) and WRF-Chem simulation (lower panels) during the EP1 (a,e), EP2 (b,f), EP3 (c,g) and EP4 (d,h). The thick white lines roughly outline the SCB region.

### 3 Results and Discussion

## 3.1 Impacts of SI on near-surface O<sub>3</sub> levels over the SCB

To illustrate the impacts of SIs on ambient environment, the temporospatial variations of

 $\Delta O_3$  (referring to the difference in  $O_3$  between the Base and EXPstro3 experiments) in the near-surface layer are analyzed for SCB and the surrounding regions based on the WRF-Chem simulation results of the innest domain. The ambient atmosphere of high-elevation regions is significantly influenced by  $O_3$ -rich stratosphere airflows when SI episode happens (Bracci et al., 2021; Yin et al., 2017). A similar spatial distribution pattern of  $\Delta O_3$  presents that SI aggravates  $O_3$  levels in the near-surface ambient atmosphere over Southwest China with higher  $O_3$  enhancements (exceeding 16 ppb) in the eastern TP rather than lower levels (approximately 6 ppb) over the SCB in all episodes (Fig. 4). Obviously, these results show the plateau-basin topography effects on  $\Delta O_3$  distribution over the region, and even confirm the connection between air quality changes in the adjoining polluted region of SCB and SI episodes occurring over the TP and surrounding area. Aiming to the SCB region, SI-induced near-surface  $O_3$  increments exhibit higher values during EP1 in springtime and lower values in EP4 of wintertime with a significant extension gradient of  $\Delta O_3$  levels at the western boundary. The phenomena involve downward  $O_3$  transport for SI from TP to SCB with prevailing westerlies under the distinctive terrain forcing, which will be further investigated in Sect. 3.2.

To assess the impacts of SI transport on atmospheric environmental changes over the SCB, we calculate the hourly concentrations of  $\triangle O_3$  and its relative contribution rate (RC) to near-surface  $O_3$  levels averaged in the region with the altitudes below 750 m above sea level (white line in Fig. 4). As shown in Fig. 5, stratospheric  $O_3$  transport affects the SCB region during the periods of 13–17 April, 1–3 July, 26–28 October and 29–30 January, with the averaged near-surface ozone enhancements of 6.3 ppb, 5.5 ppb, 4.3 ppb and 3.1 ppb, contributing 18.2%, 15.4%, 12.7% and 17.0% to regional near-surface  $O_3$  concentrations. It should be pointed out that there exist two SI episodes happened in the TP during our study period of EP1 respectively on 11 April and 15 April (Fig. 1), leading to persistent  $\triangle O_3$  transport contribution for SI during 13–18 April over the SCB. A diurnal fluctuation appears in the SI episodes with higher  $\triangle O_3$  levels in the daytime and lower those during the nighttime, reflecting the impacts of vertical mixing within atmospheric boundary layer on downward  $O_3$  transport. The East Asian monsoons significantly modulate the seasonality of near-surface  $O_3$  over the SCB region, leading to high levels and frequent  $O_3$  pollution during the warm seasons (spring and summer)

(Gao et al., 2020; Wang et al., 2022). It is noteworthy that the SCB experienced O<sub>3</sub> pollution during the EP1 and EP2 episodes. As shown in Fig. S4, the site-observed near-surface O<sub>3</sub> concentrations averaged over SCB were respectively 152.8 µm m<sup>-3</sup> for EP1 episode and 157.8 μm m<sup>-3</sup> for EP2 episode with peaks of daily maximum 8-h average ozone concentrations of 219.0 μm m<sup>-3</sup> and 233.6 μm m<sup>-3</sup>. The ozone of SI induces O<sub>3</sub> pollution aggravation in the SCB with an extra contribution of approximately 11.1-16.0%. Previous studies indicate that the unique topography of SCB amplifies the synergy effects of meteorology and emission on photochemical O<sub>3</sub> formation, dominating regional near-surface O<sub>3</sub> pollution (Yang et al., 2020; Xu et al., 2025; Wei et al., 2025). In this case study, we find the contribution of SI to nearsurface O<sub>3</sub> levels is comparable to that from transboundary transport of tropospheric O<sub>3</sub> (Shen et al., 2022). The results highlight the non-negligible impact of SI on SCB's atmospheric environment and thereby deserve more concern on the control of air pollution in the region. We acknowledge that quantifying SI contributions based on four case studies imposes inherent limitations in generalizability. While these events reveal significant SI impacts on regional air quality changes, future multi-year analyses integrating climatological SI frequencies are needed in further study on the SI contributions derived from observations and simulations.

261

262

263

264

265

266

267

268

269

270

271

272

273

274

275

276

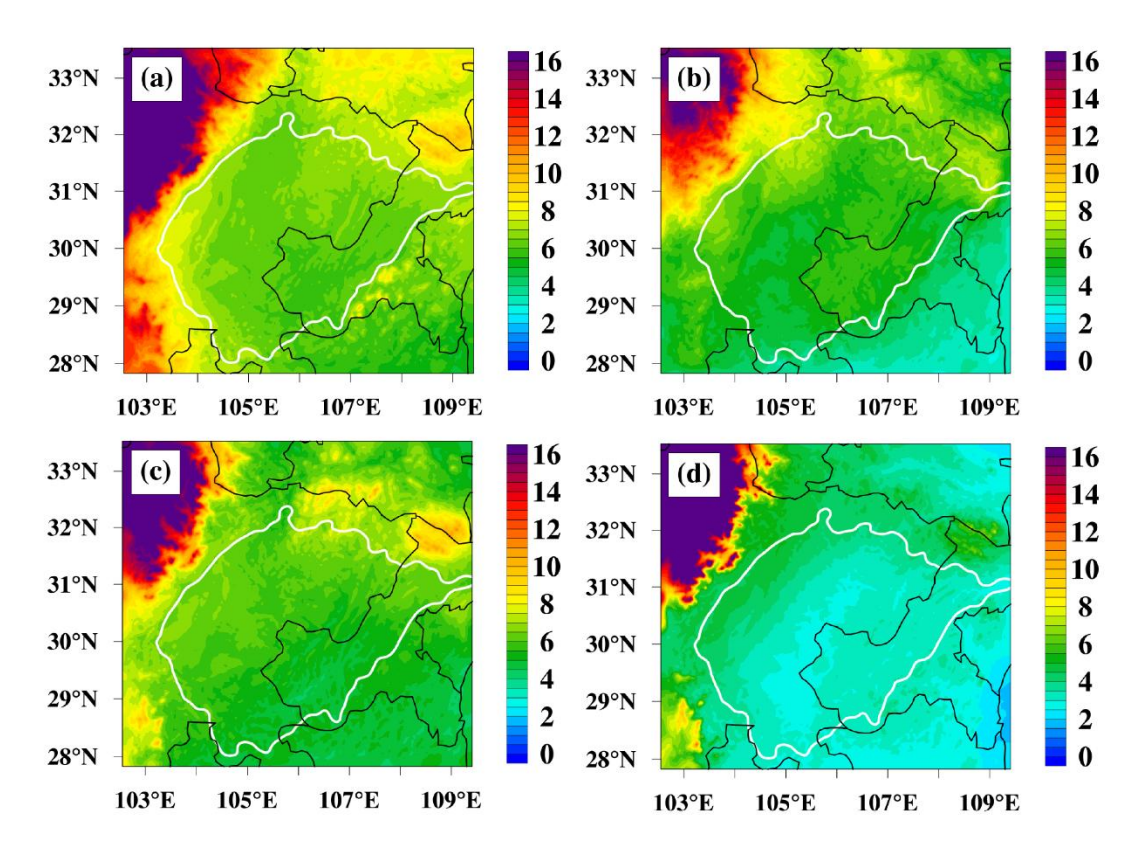


Fig  $\underline{4}$ . Spatial distribution of near-surface  $\triangle O_3$  (ppb, color contours) during SI events (a) EP1, (b) EP2, (c) EP3 and (d) EP4. The thick white lines roughly outline the SCB region.

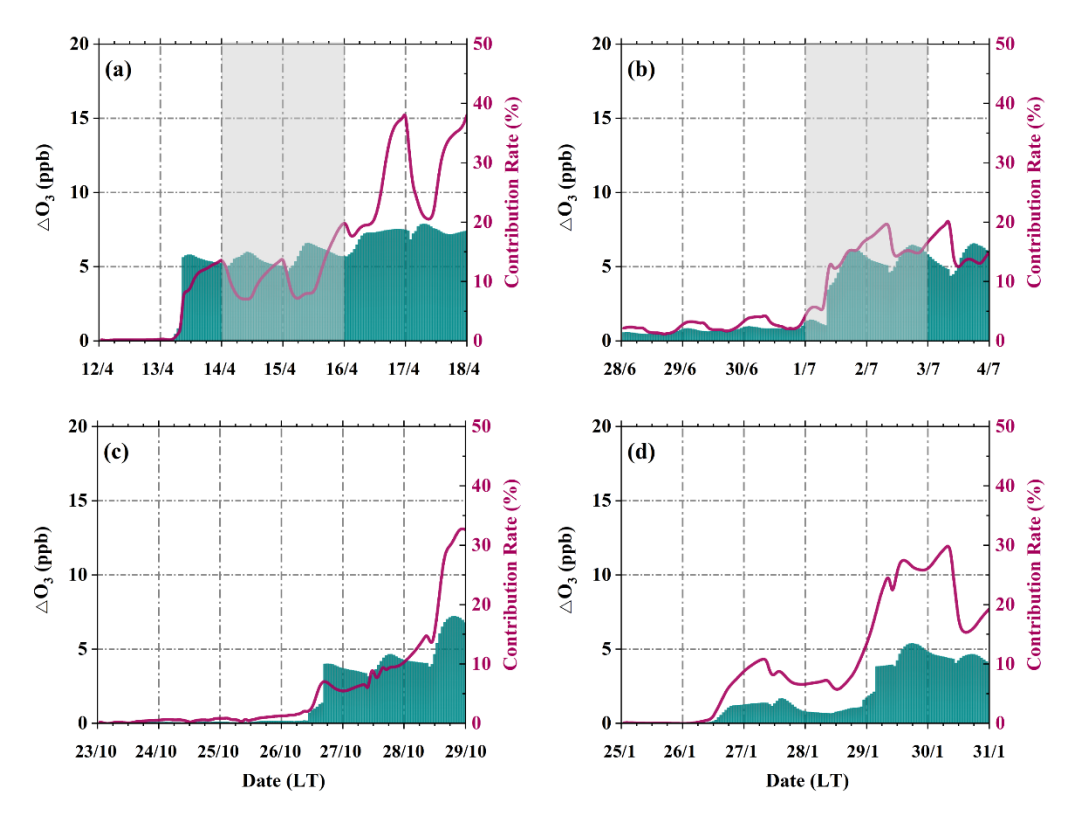


Fig  $\underline{5}$ . Hourly variations of near-surface  $\triangle O_3$  (ppb, blue-filled areas) during the period of SI events (a) EP1, (b) EP2, (c) EP3 and (d) EP4 with its relative contribution proportions (RC) to the ambient

atmosphere (dark red curve) averaged over the SCB. The gray shade indicates the regional O<sub>3</sub> pollution period.

285 286

287

288

289

290

291

292

293

294

295

296

297

298

299

300

301

302

303

304

305

306

307

308

309

310

311

312

313

284

# 3.2 Terrain-forced atmospheric circulations driving downward transport of stratospheric O<sub>3</sub>

Now that the impacts of SI on near-surface O<sub>3</sub> levels over the SCB have been estimated above, we further address the question of how atmospheric circulations persistently drive the airflows descent process across tropopause and atmospheric boundary layer simultaneously. In particular, the seasonal variations in large-topography thermodynamic and mechanical forcing of TP and SCB affect multi-scale atmospheric circulation coupling, establishing unique transport pathways from the stratosphere to near-surface atmosphere of SCB in common.

### 3.2.1 Mechanisms of SI occurrence

Seasonal variations in atmospheric circulation patterns at 200 hPa are investigated during the SIs' initial phase (Fig. 6). The results indicate that SI occurrence in the TP and surrounding regions is strongly related to the South Asian High (SAH) and subtropical jet stream activity. During the SI periods of EP1 and EP2, intense sensible heating over the elevated topography of Iranian plateau and TP induces deep convection with deep atmospheric boundary layer extending to the upper troposphere. A pronounced anticyclonic circulation, the South Asian High (SAH), is set up at 200 hPa over the Northern Hemisphere with the deepening of the westerly ridge and trough on the zonal airflow intersection. The SAH triggers SI through two dynamical processes involving: 1. anticyclone-driven peripherial subsidence: The anticyclonic circulation of SAH generates strong divergent airflows along its eastern periphery, forcing large-scale subsidence (Fig. 7a) that entrains stratospheric O<sub>3</sub> into the upper troposphere (Yang et al., 2025); 2. Rossby wave breaking (RWB) with tropopause folding (Wang et al., 2025): anticyclone-enhanced vertical wind shear initiates RWB, fragmenting the tropopause folds that inject stratospheric air into the troposphere. Anticyclonic anomalies of SAH in the upper troposphere and lower stratosphere strengthen the northern branches of the westerly jet (Yang et al., 2025) on deepening the westerly trough for deep SI events and transporting high-latitude O<sub>3</sub>-rich air intruding into the troposphere (Fig. 6), which affects lower-troposphere O<sub>3</sub> changes over the downstream East Asian region (Wang et al., 2020; Zhang et al., 2022). As shown in Fig. 6, Iranian High, one part of the SAH, exhibits an anticyclonic circulation on the western side of TP during EP1, while the summertime TP's dynamical pumping (Fig. 2) reinforces SAH evolution controlling TP region (with an intensity of 12,300 gpm). Coupled with the prevailing southwesterly monsoon, a cut-off trough is respectively produced over the central TP (EP1) and downstream regions (EP2). Correspondingly, strong atmospheric downdraft motion drives stratospheric air into the free troposphere with an abnormally high-level belt of potential vorticity (of ~8 PVU and ~6 PVU) over the region.

In addition, the subtropical westerly jet provides the atmospheric circulation background for the tropopause folding to trigger the SI of O<sub>3</sub> over the TP. Attributed to TP's location in the mid-latitude region, southward movement of subtropical westerly jet prevails over the TP in the wintertime, which intensifies tropopause disturbance (Sprenger et al., 2003), leading to frequent SI occurrence over the TP and its surrounding regions (Chen et al., 2011). Westerlies are seasonally strengthened from autumn to winter over the TP region with the southernward shift of the subtropical jet, which is reflected with the stronger westerlies in EP4 than those in EP3 forming a significant zonal structure of tropopause folding over the TP region (Fig. 6c and 6d), with a high-value region of potential vorticity at 200 hPa approximately with 4–7 PVU. These results reveal the seasonal patterns of atmospheric circulation triggering the SI over the TP hotspot region from large-scale anticyclonic circulation in the warm season to the subtropical jet in the cold season. It is worth noting that the anomalously high levels of potential vorticity appear in most regions over 40 °N, which is ascribed to the combination of zonal distribution of atmospheric tropopause heights and seasonal subtropical westerly jet stream shifts.

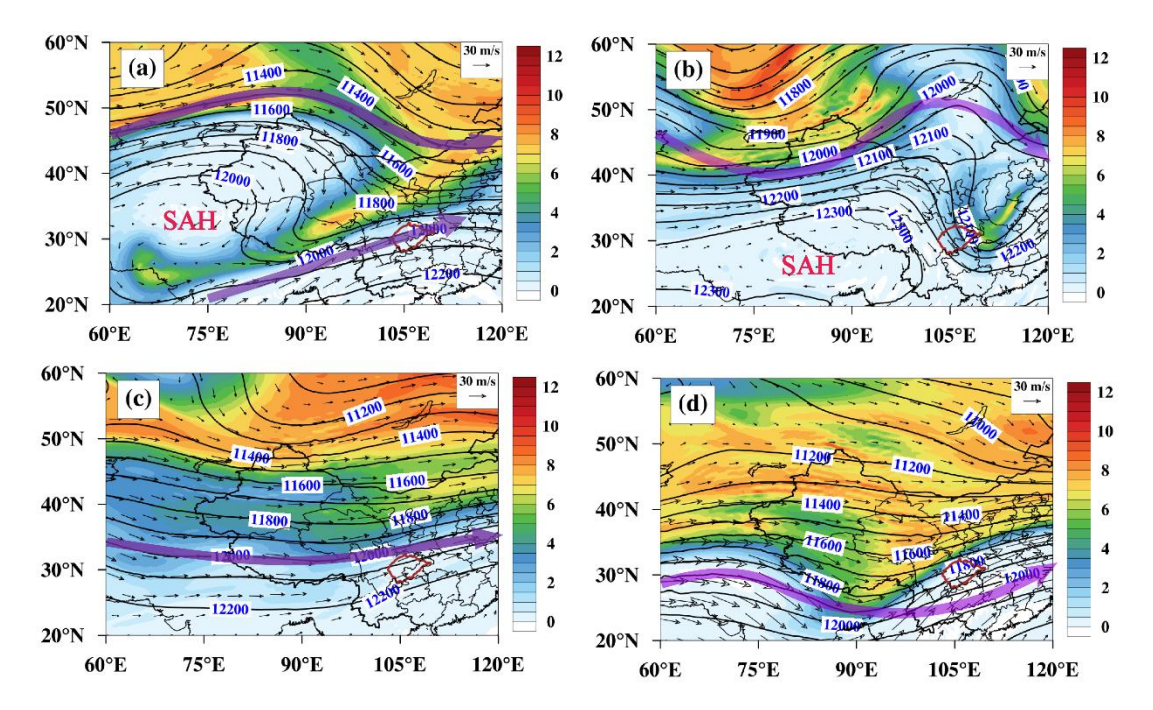


Fig <u>6</u>. Spatial distribution of geopotential height (in gpm; black lines), wind vectors and potential vorticity (units in PVU, 10<sup>-6</sup> m<sup>2</sup> s<sup>-1</sup> K kg<sup>-1</sup>; color shaded) <u>with subtropical westerly jet (purple lines with arrows)</u> at 200 hPa during (a) 15 April, (b) 1 July, (c) 26 October and (d) 28 January in 2017. The SAH indicates the South Asian High in the upper troposphere, and the red contour mark the <u>SCB-region</u>.

### 3.2.2 Stratospheric O<sub>3</sub> transport from free troposphere to near-surface atmosphere

Accompanied by high-level O<sub>3</sub> of SI entering the middle troposphere, the subsidence momentum at the eastern slope of TP keeps downward transport into the lower troposphere over the SCB. Fig. 7 shows that a similar atmospheric circulation pattern is manifested at 500 hPa during SI episodes with propagation of ridge and trough from the upper troposphere (Fig. 6). In EP1 and EP2, deepened geopotential ridges steer high-latitude cold air southward intrusion with intense subsidence in the middle-level troposphere of SCB. Whereas during the periods of EP3 and EP4 episodes, relatively straight free-troposphere westerlies are forcedly elevated at the windward slope of western TP region, while sinking airflows occur at the leeside slope of plateau over the eastern TP and downstream SCB due to the mechanical forcing of TP's large topography. That is, although there is a significant seasonal discrepancy in atmospheric circulation in the middle and upper troposphere, rich O<sub>3</sub> originating from SI is inevitably injected into the lower troposphere over SCB through the coupling effects of atmospheric vertical movements under the distinctive terrain forcing of TP.

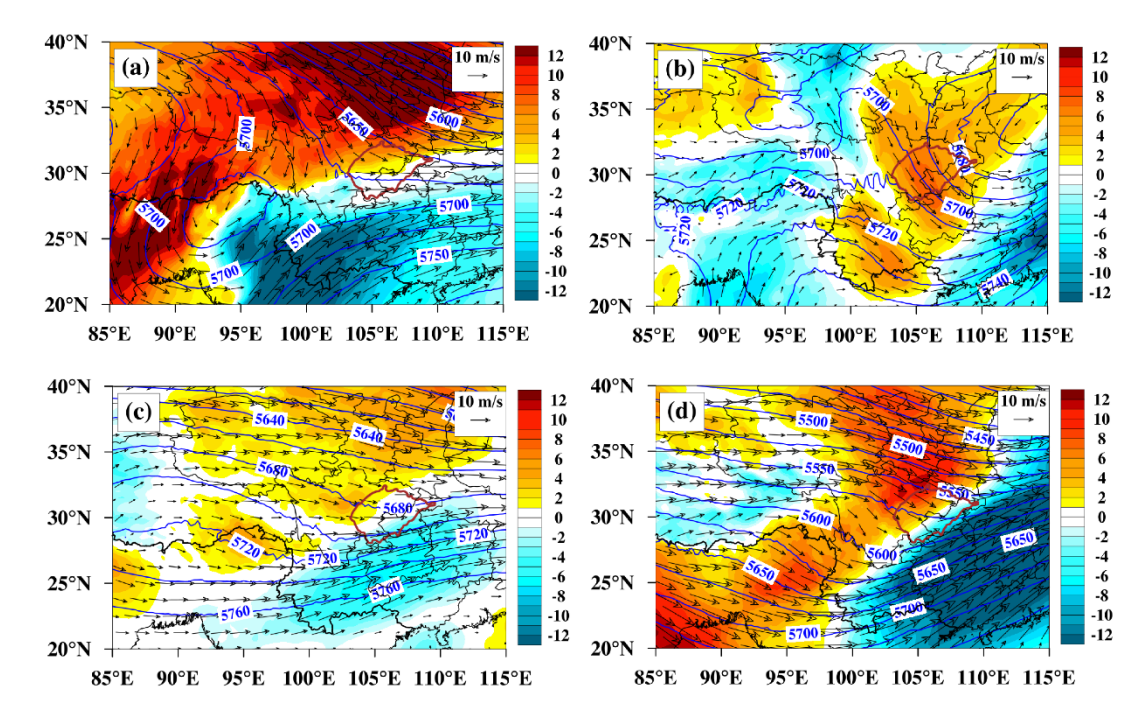


Fig <u>7</u>. Geopotential height (in gpm; blue contours), wind vectors and vertical velocity (pa s<sup>-1</sup>; shaded <u>contours</u>) at 500 hPa on (a) 16 April, (b) 1 July, (c) 26 October and (d) 29 January 2017. <u>Positive values of vertical velocity denote subsidence.</u>

The regional atmospheric structure over SCB is strongly subject to downdraft at TP's leeside slope (Xu et al., 2016, Shu et al., 2022), where vertical circulation configuration is characterized by the free-troposphere downdraft westerlies and easterly Asian monsoon within the atmospheric boundary layer, constructing a large-scale vertical wind shear and vertical vortices (Ning et al., 2019; Shu et al., 2021). The interaction of regional circulations is conducive to cross-layer exchanges of air pollutants over the SCB (Shu et al., 2023).

Fig. 8 shows the lower-troposphere vertical circulation patterns with their impacts on the downward transport of SI to the near-surface layer in SCB. Subsidence momentum dominates the SCB region driving high levels of  $O_3$  in the middle troposphere to expand into the near-surface atmosphere, with a remarkable vertical  $\triangle O_3$  difference from the height of 5 km to the near-surface layers of approximately 20 ppb.

There are two primary intrusion pathways directly and indirectly affecting air quality in the SCB for SI O<sub>3</sub>-rich airflows (Fig. 8). The direct SI pathway is vertically downwind injection of  $\triangle$  O<sub>3</sub> from the free troposphere into atmospheric boundary layer, which is related to entrainment at the top of boundary layer (Škerlak et al., 2019), mainly over the central and

eastern regions of SCB. In comparison, the indirect strtopsheric O<sub>3</sub> intrusion over the TP occurs with the slant transport pathway in the troposphere from the TP along the plateau-basin downslope into the western SCB. It is a quasi-horizontal transport process within the atmospheric boundary layer from the high-altitude eastern TP to western SCB, which results in a discernible horizontal gradient of ΔO<sub>3</sub> expansion to the west of SCB (Fig. 4). Consistent with these patterns, IPR analysis further confirms that horizontal transport dominates ΔO<sub>3</sub> changes over the plateau-basin transition zone in western SCB, whereas vertical transport drives near-surface O<sub>3</sub> increases over the flat central and eastern regions during SI episodes. Notably, the dominant transport pathway exhibits significant seasonal variability: the direct intrusion pathway prevails during the warm-season episodes EP2 and EP3, while the indirect pathway dominates during the cold-season episodes EP1 and EP4. This seasonal shift underscores the modulation of TP's topography on SI-induced O<sub>3</sub> pollution over the SCB with atmospheric circulation variations.

Another notable feature is Asian Monsoon circulation with intensified easterly wind vectors over the SCB in both EP2 and EP4, facilitating cross-layer transport of SI O<sub>3</sub> by vertical vortex in EP2 and EP4 below the heights of 3 km and 2 km (a.s.l.). These mechanisms highlight the pivotal role of the plateau-basin topography in regulating the O<sub>3</sub> transport from free troposphere to the boundary layer during SI events. The thermodynamic forcing of this topography enhances both vertical and horizontal exchange between the free troposphere and atmospheric boundary layer, critically affecting the seasonal variations of stratospheric O<sub>3</sub> intrusion.

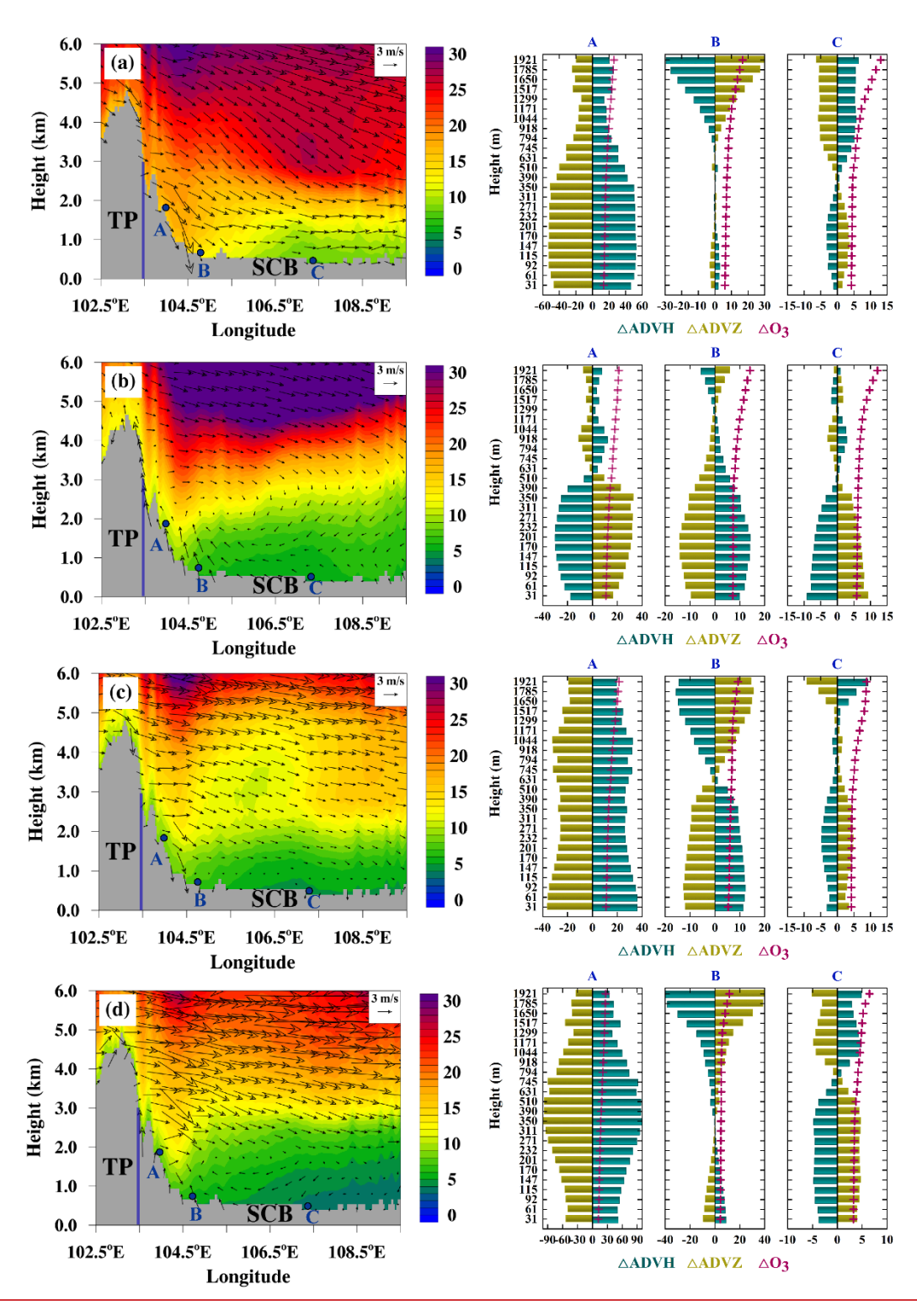


Fig <u>8</u>. Height-longitude cross-sections of  $\triangle O_3$  (ppb, color contours) and wind vectors averaged between 28–33°N on (a) 16 April, (b) 1 July, (c) 26 October and (d) 29 January 2017 (left panel) with correspondingly IPR on horizontal transport ( $\triangle ADVH$ ) and vertical transport ( $\triangle ADVZ$ ) respectively at points A (plateau region), B (western edge of SCB) and C (central SCB). The blue lines roughly outline TP's boundary.

# 3.2.3 The role of deep-basin structure in SI into ambient atmosphere

Based on the terrain sensitivity experiments (\$\Delta O\_{3basin}\$ = EXP\_{terr}\$ - EXP\_{stro3+terr}\$), we have further investigated the effect of deep-basin terrain on SI-induced near-surface O<sub>3</sub> increments. The results of \$\Delta O\_{3basin}\$ are mainly analyzed on cross-layer O<sub>3</sub> transport from the free troposphere to the near-surface atmosphere during SI episodes. We found that the low-lying basin of SCB can mitigate O<sub>3</sub> pollution derived from SIs compared to the idealized experiments with basin-filling terrain. As shown in Fig. S5 in the Supplementary information, westerlies straightly penetrate the regional atmospheric boundary layer of SCB region with stronger quasi-horizontal transboundary transport of TP's rich stratospheric O<sub>3</sub>. It would aggravate SI-induced O<sub>3</sub> enhancements over the SCB's ambient atmosphere, with averages of 9.1 ppb (EP1), 7.8 ppb (EP2), 6.6 ppb (EP3) and 8.0 ppb (EP4), respectively corresponding to the increments of 44.4 %, 41.8 %, 53.5 % and 158.1 % compared to real deep-basin topography. These results illustrate that TP modulates stratospheric O<sub>3</sub> transport between the free troposphere and ambient atmosphere while the deep-basin structure of SCB varies O<sub>3</sub> transport patterns over the region, revealing an essential terrain-forced mechanism of large plateau-basin topography on cross-layer SI transport.

### 4 Conclusion and Discussions

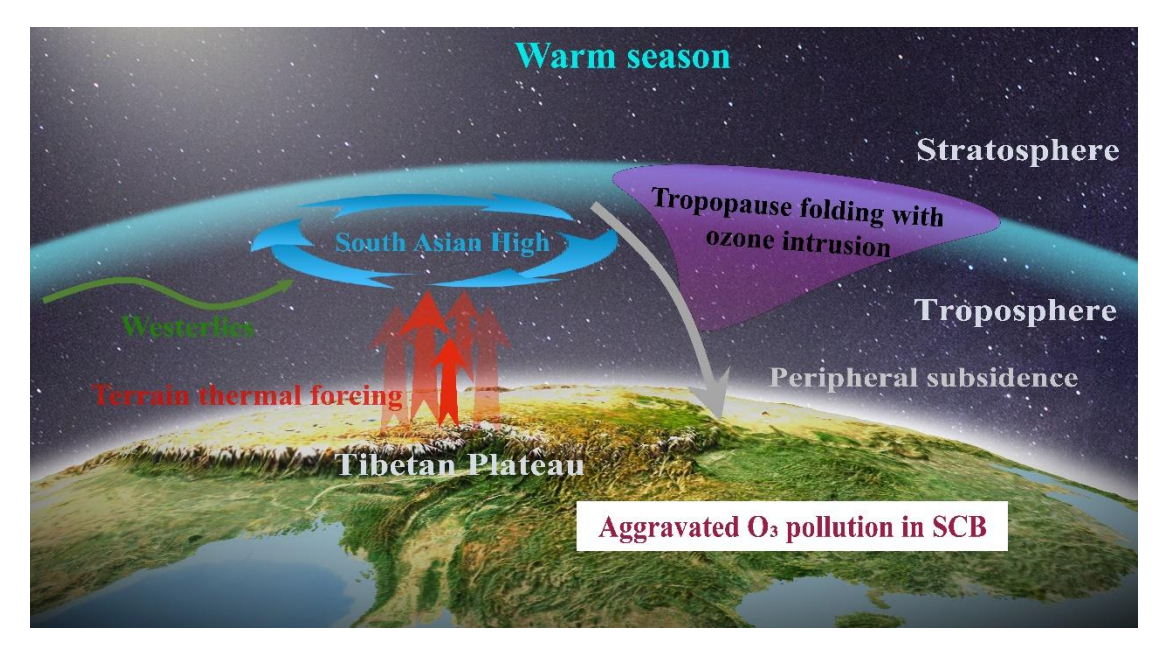
Aiming at the global SI hotspot TP (Škerlak et al., 2014) and adjoining typical polluted SCB regions, multiple-source meteorology-environment observational and reanalysis data coupled with WRF-Chem simulations are employed to quantify the impacts of stratospheric O<sub>3</sub> intrusion on the near-surface <u>ambient atmosphere</u> over SCB in the study. Four SI episodes are targeted to investigate multi-scale atmospheric circulation coupling mechanisms and their seasonality on cross-layer transport of stratospheric O<sub>3</sub> under distinctive plateau-basin terrain forcing. Results can deepen the understanding of regional O<sub>3</sub> pollution genesis with the exceptional natural sources contribution derived from the stratosphere.

The occurrence of SI in the TP and surrounding regions exerts a non-negligible impact on aggravating near-surface  $O_3$  levels over the downstream SCB, which is primarily characterized by the horizontal expansion of SI-derived  $O_3$  levels from the west edge of SCB to central region. Such downward  $O_3$  transport contributes an average increase of  $\sim$ 8.0 ppb, contributing  $\sim$ 38.7%

of environmental changes in the SCB. Larger SI-induced near-surface O<sub>3</sub> increments appear during EP1 and EP2 episodes respectively in April and July, providing an extra contribution of 11.1–16.0 % to regional O<sub>3</sub> pollution formation over the SCB. The results reveal the cross-layer O<sub>3</sub> transport affecting air quality from stratosphere to the free troposphere and ultimately into atmospheric boundary layer.

Whereafter, we explore seasonal terrain-forcing atmospheric circulation coupling mechanisms on cross-layer O<sub>3</sub> transport. Fig. 9 summarizes the primary triggering effects as follows: The unique plateau's thermodynamic forcing in warm seasons but mechanical forcing in the cold season respectively modulates stratospheric O<sub>3</sub>-rich air injection into the nearsurface atmosphere over the SCB affecting regional air quality. On one hand, the joint thermal forcing of TP and Iranian Plateau in EP1 and EP2 triggers stratospheric O3 intrusion over the TP and surrounding regions by peripheral subsidence of South Asian High in the upper troposphere. Stratospheric O<sub>3</sub> is steered by intensified zonal interaction of westerlies driving high-latitude cold airflows downward transport into the adjacent SCB region. On the other hand, the southward retreat of subtropical jet stream during the EP3 and EP4 leads to SIs occurrence over the TP (Chen et al., 2011; Luo et al., 2019). With the TP's mechanical forcing on stronger middle-troposphere westerlies, leeward slope subsidence deliver high-level stratospheric O<sub>3</sub> to the lower troposphere over the SCB region. Two primary pathways are identified to affect air quality over the SCB for SI-derived O<sub>3</sub>, involving along the TP's downslope into the western SCB and directly downwind transport into atmospheric boundary layer over the central and eastern regions of SCB. The existence of low-lying deep basin structure weakens the contribution of SI to ambient atmosphere in the SCB.

This modeling study investigats the four episodes for a seasonal assessment of the contribution of stratospheric O<sub>3</sub> intrusion to the SCB regions in Southwest China, highlighting the multi-scale atmospheric circulation coupling mechanisms under the distinctive plateaubasin terrain forcing. In the future, it is necessary to generalize the climatology of SI impacts on near-surface environmental atmosphere in the region with multi-year observations and simulations.



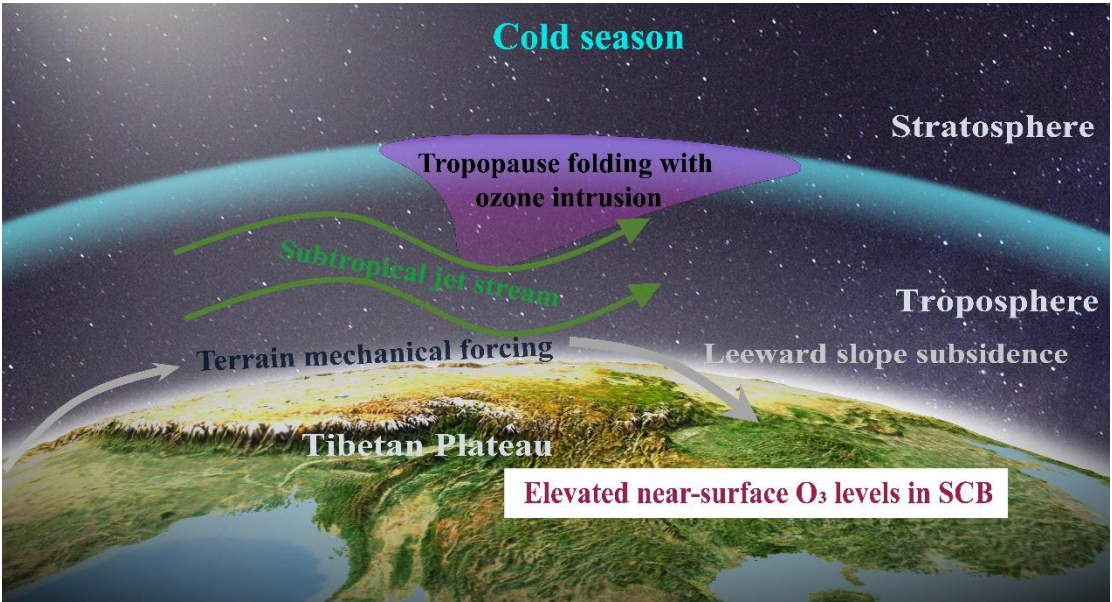


Fig <u>9</u>. Diagram on the cross-layer transport of stratospheric O<sub>3</sub> on regional atmospheric environmental changes over SCB driven by mult-scale atmospheric circulation pattern with the seasonally discrepant terrain effects of TP.

# Data availability

The ground-based environment and meteorology data are respectively available at the China National Environmental Monitoring Center (<a href="http://www.cnemc.cn/">http://www.cnemc.cn/</a>) and the Chinese Meteorological Monitoring Network (<a href="http://data.cma.cn/">http://data.cma.cn/</a>). ERA5 data are derived from Copernicus Climate Change Service (C3S) Climate Date Store (<a href="https://cds.climate.copernicus.eu/datasets">https://cds.climate.copernicus.eu/datasets</a>). EAC4 reanalysis data are obtained from Copernicus Atmosphere Monitoring Service (<a href="https://ads.atmosphere.copernicus.eu/datasets">https://ads.atmosphere.copernicus.eu/datasets</a>).

- 474 All data used in this paper can be provided upon request from Zhuozhi Shu
- 475 (shuzhuozhi@foxmail.com).

### 476 **Author Contributions**

- 477 Conceptualization: ZS, TZ, FY, GS, YZ. Investigation: ZS, YH, XY, BP. Methodology: ZS, TZ,
- 478 YZ. Validation: YH, XY, BP. Writing (original draft preparation): ZS, TZ, YZ. Writing (review and
- editing): ZS, TZ, YZ, FY, GS. All of the authors provided commentary on the paper.

## **Competing interest**

480

482

The authors declare that they have no conflict of interest.

## Acknowledgments

- This work was supported jointly by the National Natural Science Foundation of China (Grant No.
- 484 42405195 and 42275196), the National Key Research and Development Program of China (Grant
- No. 2022YFC3701204 and 2023YFC3709301) and the National Natural Science Foundation of
- 486 China (Grant No. 42207134 and 42465008).

### 487 **References**

- Barth, M. C., Lee, J., Hodzic, A., Pfister, G., Skamarock, W. C., Worden, J., Wong, J., and Noone, D.:
- 489 Thunderstorms and upper troposphere chemistry during the early stages of the 2006 North American
- 490 Monsoon. Atmospheric Chemistry and Physics, 12, 11003-11026. https://doi.org/10.5194/acp-12-
- 491 <u>11003-2012</u>, 2012.
- Bracci, A., Cristofanelli, P., Sprenger, M., Bonafè, U., Calzolari, F., Duchi, R., Laj, P., Marinoni, A.,
- 493 Roccato, F., Vuillermoz, E., and Bonasoni, P.: Transport of Stratospheric Air Masses to the Nepal Climate
- 494 Observatory-Pyramid (Himalaya; 5079 m MSL): A Synoptic-Scale Investigation. Journal of Applied
- 495 Meteorology and Climatology, 51, 1489–1507. https://doi.org/10.1175/JAMC-D-11-0154.1, 2012.
- Brewer, A.W.: Evidence for a world circulation provided by the measurements of helium and water
- 497 vapour distribution in the stratosphere. Quarterly Journal of the Royal Meteorological Society, 75, 351–
- 498 363. https://doi.org/10.1002/qj.49707532603, 1949.
- 499 Butchart, N.: The Brewer-Dobson circulation. Reviews of Geophysics, 52, 157-184.
- 500 https://doi.org/10.1002/2013RG000448, 2014.
- 501 Chen, X., Ma, Y., Kelder, H., Su, Z., and Yang, K.: On the behaviour of the tropopause folding events
- 502 over the Tibetan Plateau. Atmospheric Chemistry and Physics, 11, 5113-5122.
- 503 <u>https://doi.org/10.5194/acp-11-5113-2011</u>, 2011.
- Chen, Z., Liu, J., Cheng, X., Yang, M., and Shu, L.: Stratospheric influences on surface ozone increase
- during the COVID-19 lockdown over northern China. npj Climate and Atmospheric Science, 6, 76.
- 506 https://doi.org/10.1038/s41612-023-00406-2, 2023.
- 507 Chou, Y., Huang, Q., Zhang, Yongpeng, Luo, J., Wang, M., Liao, H., Zhang, Y., and Bai, Z.: Impacts of
- deep boundary layer on near-surface ozone concentration over the Tibetan Plateau. Atmospheric

- 509 Environment, 294, 119532. https://doi.org/10.1016/j.atmosenv.2022.119532, 2023.
- 510 Ding, A., and Wang, T.: Influence of stratosphere-to-troposphere exchange on the seasonal cycle of
- 511 surface ozone at Mount Waliguan in western China. Geophysical Research Letters, 33, L03803.
- 512 https://doi.org/10.1029/2005GL024760, 2006.
- 513 Dobson, G. M. B.: Origin and distribution of the polyatomic molecules in the atmosphere. Proceedings
- 814 Royal Society Lond. A, 236, 187–193. https://doi.org/10.1098/rspa.1956.0127, 1956.
- 515 Duan, A., and Wu, G.: Weakening Trend in the Atmospheric Heat Source over the Tibetan Plateau during
- 516 Recent Decades. Part I: Observations. Journal of Climate, 21, 3149-3164.
- 517 https://doi.org/10.1175/2007JCLI1912.1, 2008.
- Emery, C.A., Tai, E., and Yarwood, G.: Enhanced Meteorological Modeling and Performance Evaluation
- for Two Texas Ozone Episodes. Prepared for the Texas Natural Resource Conservation Commission, by
- 520 Environ International Corp. https://api.semanticscholar.org/CorpusID:127579774, 2001.
- Feng, Z., Hu, E., Wang, X., Jiang, L., and Liu, X.: Ground-level O<sub>3</sub> pollution and its impacts on food
- 522 crops in China: A review. Environmental Pollution, 199, 42–48.
- 523 <u>https://doi.org/10.1016/j.envpol.2015.01.016</u>, 2015.
- Fiore, A. M., Jacob, D. J., Field, B. D., Streets, D. G., Fernandes, S. D., and Jang, C.: Linking ozone
- 525 pollution and climate change: The case for controlling methane. Geophysical Research Letter,s 29, 25-
- 526 1-25–4. https://doi.org/10.1029/2002GL015601, 2002.
- 527 Fu, R., Hu, Y., Wright, J. S., Jiang, J. H., Dickinson, R. E., Chen, M., Filipiak, M., Read, W. G., Waters,
- J. W., and Wu, D. L.: Short circuit of water vapor and polluted air to the global stratosphere by convective
- transport over the Tibetan Plateau. Proceedings of the National Academy of Sciences, 103, 5664–5669.
- 530 https://doi.org/10.1073/pnas.0601584103, 2006.
- 531 Gao, M., Gao, J., Zhu, B., Kumar, R., Lu, X., Song, S., Zhang, Y., Jia, B., Wang, P., Beig, G., Hu,
- J., Ying, Q., Zhang, H., Sherman, P., McElroy, M.B.: Ozone pollution over China and India:
- 533 seasonality and sources. Atmos. Chem. Phys. 20 (7), 4399–4414. https://doi.org/10.5194/acp-20-
- 534 4399-2020, 2020.
- Guenther, A. B., Jiang, X. and Heald, C. L., Sakulyanontvittaya, T., Duhl, T., Emmons, L. K., and Wang,
- 536 X. The Model of Emissions of Gases and Aerosols from Nature version 2.1 (MEGAN2.1): an extended
- 537 and updated framework for modeling biogenic emissions. Geoscientific Model Development, 5, 1471-
- 538 1492. https://doi.org/10.5194/gmd-5-1471-2012, 2012.
- 539 Hu, J., Zhao, T., Liu, J., Cao, L., Wang, C., Li, Y., Shi, C., Tan, C., Sun, X., Shu, Z., and Li, J.: Exploring
- 540 the ozone pollution over the western Sichuan Basin, Southwest China: The impact of diurnal change in
- 541 mountain-plains solenoid. Science of the Total Environment, 839, 156264.
- 542 <u>https://doi.org/10.1016/j.scitotenv.2022.156264</u>, 2022.
- Huang, J., Zhou, X., Wu, G., Xu, X., Zhao, Q., Liu, Yimin, Duan, A., Xie, Y., Ma, Y., Zhao, P., Yang, S.,
- Yang, K., Yang, H., Bian, J., Fu, Y., Ge, J., Liu, Yuzhi, Wu, Q., Yu, H., and Qie, K.: Global Climate
- 545 Impacts of Land-Surface and Atmospheric Processes Over the Tibetan Plateau. Reviews of Geophysics,
- 546 61. https://doi.org/10.1029/2022RG000771, 2023.
- 547 Inness, A., Ades, M., Agustí-Panareda, A., Barré, J., Benedictow, A., Blechschmidt, A.-M., Dominguez,
- J.J., Engelen, R., Eskes, H., Flemming, J., Huijnen, V., Jones, L., Kipling, Z., Massart, S., Parrington, M.,
- Peuch, V.-H., Razinger, M., Remy, S., Schulz, M., and Suttie, M.: The CAMS reanalysis of atmospheric
- composition. Atmospheric Chemistry and Physics, 19, 3515–3556. https://doi.org/10.5194/acp-19-3515-
- 551 <u>2019</u>, 2019.
- Kong, L., Zhou, L., Chen, D., Luo, L., Xiao, K., Chen, Y., Liu, H., Tan, Q., and Yang, F.: Atmospheric

- 553 oxidation capacity and secondary pollutant formation potentials based on photochemical loss of VOCs
- 554 in a megacity of the Sichuan Basin, China. Science of the Total Environment, 901, 166259.
- 555 https://doi.org/10.1016/j.scitotenv.2023.166259, 2023.
- Koumoutsaris, S., Bey, I., Generoso, S., and Thouret, V.: Influence of El Niño-Southern Oscillation on
- 557 the interannual variability of tropospheric ozone in the northern midlatitudes. Journal of Geophysical
- 558 Research: Atmospheres, 113. <a href="https://doi.org/10.1029/2007JD009753">https://doi.org/10.1029/2007JD009753</a>, 2008.
- Lamarque, J.-F., Emmons, L. K., Hess, P. G., Kinnison, D. E., Tilmes, S., Vitt, F., Heald, C. L., Holland,
- 560 E. A., Lauritzen, P. H., Neu, J., Orlando, J. J., Rasch, P. J., and Tyndall, G. K.: CAM-chem: description
- and evaluation of interactive atmospheric chemistry in the Community Earth System Model.
- 562 Geoscientific Model Development, 5, 369–411. https://doi.org/10.5194/gmd-5-369-2012, 2012.
- Lee, J., Wu, Y., and Wang, X.: The evolutions and large-scale mechanisms of summer stratospheric ozone
- 564 intrusion across global hotspots. Journal of Geophysical Research: Atmospheres, 129(4),
- 655 e2023JD039877. https://doi.org/10.1029/2023JD039877, 2024.
- Li, D., Vogel, B., Müller, R., Bian, J., Günther, G., Li, Q., Zhang, J., Bai, Z., Vömel, H., and Riese, M.:
- 567 High tropospheric ozone in Lhasa within the Asian summer monsoon anticyclone in 2013: influence of
- 568 convective transport and stratospheric intrusions. Atmospheric Chemistry and Physics, 18, 17979–17994.
- 569 https://doi.org/10.5194/acp-18-17979-2018, 2018.
- Lin, M., Fiore, A. M., Cooper, O. R., Horowitz, L. W., Langford, A. O., Levy II, H., Johnson, B. J., Naik,
- V., Oltmans, S. J., and Senff, C. J.: Springtime high surface ozone events over the western United States:
- Quantifying the role of stratospheric intrusions. Journal of Geophysical Research: Atmospheres, 117.
- 573 https://doi.org/10.1029/2012JD018151, 2012.
- Lin, M., Fiore, A. M., Horowitz, L. W., Langford, A. O., Oltmans, S. J., Tarasick, D., and Rieder, H. E.:
- 575 Climate variability modulates western US ozone air quality in spring via deep stratospheric intrusions.
- 576 Nature Communications, 6, 7105. <a href="https://doi.org/10.1038/ncomms8105">https://doi.org/10.1038/ncomms8105</a>, 2015.
- 577 Liu, J., Strode, S. A., Liang, Q., Oman, L. D., Colarco, P. R., Fleming, E. L., Manyin, M. E., Douglass,
- 578 A. R., Ziemke, J. R., Lamsal, L. N., and Li, C.: Change in Tropospheric Ozone in the Recent Decades
- and Its Contribution to Global Total Ozone. Journal of Geophysical Research: Atmospheres, 127,
- 580 e2022JD037170. https://doi.org/10.1029/2022JD037170, 2022.
- Lu, X., Hong, J., Zhang, L., Cooper, O. R., Schultz, M. G., Xu, X., Wang, T., Gao, M., Zhao, Y., and
- Zhang, Y.: Severe Surface Ozone Pollution in China: A Global Perspective. Environmental Science &
- Technology Letters, 5, 487–494. <a href="https://doi.org/10.1021/acs.estlett.8b00366">https://doi.org/10.1021/acs.estlett.8b00366</a>, 2018.
- Luo, J., Liang, W., Xu, P., Xue, H., Zhang, M., Shang, L., and Tian, H.: Seasonal Features and a Case
- 585 Study of Tropopause Folds over the Tibetan Plateau. Advances in Meteorology, 2019, 1-12.
- 586 <a href="https://doi.org/10.1155/2019/4375123">https://doi.org/10.1155/2019/4375123</a>, 2019.
- Ma, J., Lin, W. L., Zheng, X., Xu, X., Li, Z., and Yang, L.: Influence of air mass downward transport on
- 588 the variability of surface ozone at Xianggelila Regional Atmosphere Background Station, southwest
- 589 China. Atmospheric Chemistry and Physics, 14, 5311–5325. https://doi.org/10.5194/acp-14-5311-2014,
- 590 2014.
- Miri, M., Derakhshan, Z., Allahabadi, A., Ahmadi, E., Oliveri Conti, G., Ferrante, M., and Aval, H. E.:
- Mortality and morbidity due to exposure to outdoor air pollution in Mashhad metropolis, Iran. The AirQ
- 593 model approach. Environmental Research, 151, 451–457. https://doi.org/10.1016/j.envres.2016.07.039,
- 594 2016.
- Monks, P. S., Archibald, A. T., Colette, A., Cooper, O., Coyle, M., Derwent, R., Fowler, D., Granier, C.,
- Law, K. S., Mills, G. E., Stevenson, D. S., Tarasova, O., Thouret, V., von Schneidemesser, E., Sommariva,

- 597 R., Wild, O., and Williams, M.L.: Tropospheric ozone and its precursors from the urban to the global
- scale from air quality to short-lived climate forcer. Atmospheric Chemistry and Physics, 15, 8889–8973.
- 599 https://doi.org/10.5194/acp-15-8889-2015, 2015.
- Neu, J. L., Flury, T., Manney, G. L., Santee, M. L., Livesey, N. J., and Worden, J.: Tropospheric ozone
- 601 variations governed by changes in stratospheric circulation. Nature Geoscience, 7, 340-344.
- 602 https://doi.org/10.1038/ngeo2138, 2014.
- Nieto, R., Gimeno, L., de la Torre, L., Ribera, P., Gallego, D., García-Herrera, R., García, J.A., Nuñez,
- 604 M., Redaño, A., and Lorente, J.: Climatological Features of Cutoff Low Systems in the Northern
- 605 Hemisphere. Journal of Climate, 18, 3085–3103. https://doi.org/10.1175/JCLI3386.1, 2005.
- Ning, G., Yim, S. H. L., Wang, S., Duan, B., Nie, C., Yang, X., Wang, J., and Shang, K.: Synergistic
- effects of synoptic weather patterns and topography on air quality: a case of the Sichuan Basin of China.
- 608 Climate Dynamics, 53, 6729–6744. https://doi.org/10.1007/s00382-019-04954-3, 2019.
- Pierce, B., and Holloway, T.: When Stratospheric Ozone Hits Ground-level Regulation: Exceptional
- 610 Events in Wyoming. Bulletin of the American Meteorological Society, 98, 889-892.
- 611 <u>https://doi.org/10.1175/BAMS-D-14-00133.1</u>, 2017.
- Prather, M. J., Zhu, X., Tang, Q., Hsu, J., and Neu, J. L.: An atmospheric chemist in search of the
- tropopause. Journal of Geophysical Research, 116, D04306. <a href="https://doi.org/10.1029/2010JD014939">https://doi.org/10.1029/2010JD014939</a>,
- 614 2011.
- Shen, L., Liu, J., Zhao, T., Xu, X., Han, H., Wang, H. and Shu, Z.: Atmospheric transport drives
- regional interactions of ozone pollution in China. Science of the Total Environment, 830, p.154634.
- 617 https://doi.org/10.1016/j.scitotenv.2022.154634, 2022.
- 618 Shu, Z., Liu, Y., Zhao, T., Xia, J., Wang, C., Cao, L., Wang, H., Zhang, L., Zheng, Y., Shen, L., Luo, L.,
- and Li, Y.: Elevated 3D structures of PM<sub>2.5</sub> and impact of complex terrain-forcing circulations on heavy
- haze pollution over Sichuan Basin, China. Atmospheric Chemistry and Physics, 21, 9253-9268.
- 621 https://doi.org/10.5194/acp-21-9253-2021, 2021.
- 622 Shu, Z., Zhao, T., Chen, Y., Liu, Y., Yang, F., Jiang, Y., He, G., Yang, Q., and Zhang, Y.: Terrain effect on
- 623 atmospheric process in seasonal ozone variation over the Sichuan Basin, Southwest China.
- 624 Environmental Pollution, 338, 122622. https://doi.org/10.1016/j.envpol.2023.122622, 2023.
- 625 Shu, Z., Zhao, T., Liu, Y., Zhang, L., Ma, X., Kuang, X., Li, Y., Huo, Z., Ding, Q., Sun, X., and Shen, L.:
- Impact of deep basin terrain on PM<sub>2.5</sub> distribution and its seasonality over the Sichuan Basin, Southwest
- 627 China. Environmental Pollution, 300, 118944. <a href="https://doi.org/10.1016/j.envpol.2022.118944">https://doi.org/10.1016/j.envpol.2022.118944</a>, 2022.
- 628 Škerlak, B., Pfahl, S., Sprenger, M., and Wernli, H.: A numerical process study on the rapid transport of
- 629 stratospheric air down to the surface over western North America and the Tibetan Plateau. Atmospheric
- 630 Chemistry and Physics, 19, 6535–6549. https://doi.org/10.5194/acp-19-6535-2019, 2019.
- 631 Škerlak, B., Sprenger, M., Pfahl, S., Tyrlis, E., and Wernli, H.: Tropopause folds in ERA-Interim: Global
- 632 climatology and relation to extreme weather events. Journal of Geophysical Research: Atmospheres, 120,
- 633 4860–4877. https://doi.org/10.1002/2014JD022787, 2015.
- 634 Škerlak, B., Sprenger, M., and Wernli, H.: A global climatology of stratosphere–troposphere exchange
- using the ERA-Interim data set from 1979 to 2011. Atmospheric Chemistry and Physics, 14, 913–937.
- 636 <u>https://doi.org/10.5194/acp-14-913-2014</u>, 2014.
- 637 Sprenger, M., Maspoli, M. C., and Wernli, H.: Tropopause folds and cross-tropopause exchange: A global
- 638 investigation based upon ECMWF analyses for the time period March 2000 to February 2001. Journal
- of Geophysical Research, 108, 8518. <a href="https://doi.org/10.1029/2002JD002587">https://doi.org/10.1029/2002JD002587</a>, 2003.
- 640 Stohl, A., Wernli, H., James, P., Bourqui, M., Forster, C., Liniger, M. A., Seibert, P., and Sprenger, M.: A

- New Perspective of Stratosphere-Troposphere Exchange. Bulletin of the American Meteorological
- 642 Society, 84, 1565–1574. https://doi.org/10.1175/BAMS-84-11-1565, 2003.
- 643 Trickl, T., Bartsch-Ritter, N., Eisele, H., and Furger, M.: High-ozone layers in the middle and upper
- troposphere above Central Europe: potential import from the stratosphere along the subtropical jet stream.
- 645 Atmospheric Chemistry and Physics, 11, 9343–9366. https://doi.org/10.5194/acp-11-9343-2011, 2011.
- Trickl, T., Vogelmann, H., Giehl, H., Scheel, H.-E., Sprenger, M., and Stohl, A.: How stratospheric are
- 647 deep stratospheric intrusions? Atmospheric Chemistry and Physics, 14, 9941-9961.
- 648 <u>https://doi.org/10.5194/acp-14-9941-2014, 2014.</u>
- Venkat Ratnam, M., Ravindra Babu, S., Das, S. S., Basha, G., Krishnamurthy, B. V., and Venkateswararao,
- B.: Effect of tropical cyclones on the stratosphere-troposphere exchange observed using satellite
- observations over the north Indian Ocean. Atmospheric Chemistry and Physics, 16, 8581-8591.
- 652 https://doi.org/10.5194/acp-16-8581-2016, 2016.
- Wang, H., Wang, W., Huang, X., and Ding, A.: Impacts of stratosphere-to-troposphere-transport on
- 654 summertime surface ozone over eastern China. Science Bulletin, 65, 276-279
- 655 <u>https://doi.org/10.1016/j.scib.2019.11.017</u>, 2020.
- 656 Wang, L., Li, M., Wang, Q., Li, Y., Xin, J., Tang, X., Du, W., Song, T., Li, T., Sun, Y., Gao, W., Hu, B.,
- and Wang, Y.: Air stagnation in China: Spatiotemporal variability and differing impact on PM<sub>2.5</sub> and O<sub>3</sub>
- 658 during 2013–2018. Science of the Total Environment, 819, 152778.
- 659 <u>https://doi.org/10.1016/j.scitotenv.2021.152778</u>, 2022.
- 660 Wang, W., Parrish, D.D., Wang, S., Bao, F., Ni, R., Li, X., Yang, S., Wang, H., Cheng, Y., Su, H.:
- 661 Long-term trend of ozone pollution in China during 2014-2020: distinct seasonal and spatial
- 662 characteristics and ozone sensitivity. Atmos. Chem. Phys. 22 (13), 8935-8949.
- https://doi.org/10.5194/acp-22-8935-2022, 2022.
- 664 Wang, N., Du, Y., Chen, D., Meng, H., Chen, X., Zhou, L., Shi, G., Zhan, Y., Feng, M., Li, W., Chen, M.,
- 665 Li, Z., and Yang, F.: Spatial disparities of ozone pollution in the Sichuan Basin spurred by extreme, hot
- 666 weather. Atmospheric Chemistry and Physics, 24, 3029–3042. https://doi.org/10.5194/acp-24-3029-2024,
- 667 2023.
- Wang, Y., He, Y., Sheng, Z., Sun, J., Qin, Z. and Tao, Y. Vertical ozone transport by Rossby wave breaking
- 669 in upper troposphere-lower stratosphere is weakening. Atmospheric Environment, 343, p.120999.
- 670 https://doi.org/10.1016/j.atmosenv.2024.120999, 2025.
- Waugh, D. W., and Polvani, L. M.: Climatology of intrusions into the tropical upper troposphere.
- 672 Geophysical Research Letters, 27, 3857–3860. https://doi.org/10.1029/2000GL012250, 2000.
- 673 Wei, J., Li, Z., Li, K., Dickerson, R. R., Pinker, R. T., Wang, J., Liu, X., Sun, L., Xue, W., and Cribb, M.:
- Full-coverage mapping and spatiotemporal variations of ground-level ozone (O<sub>3</sub>) pollution from 2013 to
- 675 2020 across China. Remote Sensing of Environment, 270, 112775.
- 676 https://doi.org/10.1016/j.rse.2021.112775, 2022.
- Wei, J., Ren, J., Li, J. and Xie, S.: Characteristics and drivers of springtime ozone pollution in the
- 678 Sichuan Basin, China, in May 2020 and 2024. Atmospheric Environment, 361, p.121476.
- 679 https://doi.org/10.1016/j.atmosenv.2025.121476, 2025.
- 680 Williams, R. S., Hegglin, M. I., Kerridge, B. J., Jöckel, P., Latter, B. G., and Plummer, D. A.:
- 681 Characterising the seasonal and geographical variability in tropospheric ozone, stratospheric influence
- and recent changes. Atmospheric Chemistry and Physics, 19, 3589–3620. https://doi.org/10.5194/acp-
- 683 <u>19-3589-2019</u>, 2019.
- Xian, Y., Zhang, Y., Liu, Z., Wang, H., Wang, J., and Tang, C.: Source apportionment and formation of

- warm season ozone pollution in Chengdu based on CMAQ-ISAM. Urban Climate, 56, 102017.
- 686 https://doi.org/10.1016/j.uclim.2024.102017, 2024.
- Kristovich, D., Lu, C., Guo, Y., Cheng, X., Wang, Y., and Ding, G.:
- 688 Climate modulation of the Tibetan Plateau on haze in China. Atmospheric Chemistry and Physics, 16,
- 689 1365–1375. https://doi.org/10.5194/acp-16-1365-2016, 2016.
- 690 Xu, T., Gao, X., Jiang, S., Hu, K., Peng, Z., Zhao, X. and Tang, X.: Nonlinear ozone response to
- 691 extreme high temperature in a subtropical megacity basin: Integrated observation and modeling
- analysis. Environmental Research, p.122274. <a href="https://doi.org/10.1016/j.envres.2025.122274">https://doi.org/10.1016/j.envres.2025.122274</a>, 2025.
- 693 Yang, J., Wang, K., Lin, M., Yin, X., and Kang, S.: Not biomass burning but stratospheric intrusion
- dominating tropospheric ozone over the Tibetan Plateau. Proceedings of the National Academy of
- 695 Sciences, 119, e2211002119. <a href="https://doi.org/10.1073/pnas.2211002119">https://doi.org/10.1073/pnas.2211002119</a>, 2022.
- 696 Yang, X., Wu, K., Wang, H., Liu, Y., Gu, S., Lu, Y., Zhang, X., Hu, Y., Ou, Y., Wang, S. and Wang,
- 697 Z.: Summertime ozone pollution in Sichuan Basin, China: Meteorological conditions, sources and
- 698 process analysis. Atmospheric Environment, 226, p.117392.
- 699 https://doi.org/10.1016/j.atmosenv.2020.117392, 2020.
- 700 Yang, Q., Zhao, T., Bai, Y., Meng, K., Luo, Y., Tian, Z., Sun, X., Fu, W., Yang, K., and Hu, J.:
- 701 Distinct structures of interannual variations in stratosphere-to-troposphere ozone transport induced
- 702 by the Tibetan Plateau thermal forcing, Atmos. Chem. Phys., 25, 8029-8042.
- 703 https://doi.org/10.5194/acp-25-8029-2025, 2025.
- Yin, X., Kang, S., de Foy, B., Cong, Z., Luo, J., Zhang, L., Ma, Y., Zhang, G., Rupakheti, D., and Zhang,
- Q.: Surface ozone at Nam Co in the inland Tibetan Plateau: variation, synthesis comparison and regional
- representativeness. Atmospheric Chemistry and Physics, 17, 11293–11311. https://doi.org/10.5194/acp-
- 707 <u>17-11293-2017</u>, 2017.
- 708 Yin, X., Rupakheti, D., Zhang, G., Luo, J., Kang, S., de Foy, B., Yang, J., Ji, Z., Cong, Z., Rupakheti, M.,
- 709 Li, P., Hu, Y., and Zhang, Q.: Surface ozone over the Tibetan Plateau controlled by stratospheric intrusion.
- 710 Atmospheric Chemistry and Physics, 23, 10137–10143. https://doi.org/10.5194/acp-23-10137-2023,
- 711 2023.
- 712 Zhang, L., Guo, X., Zhao, T., Gong, S., Xu, X., Li, Y., Luo, L., Gui, K., Wang, H., Zheng, Y., and Yin,
- 713 X.: A modelling study of the terrain effects on haze pollution in the Sichuan Basin. Atmospheric
- 714 Environment, 196, 77–85. https://doi.org/10.1016/j.atmosenv.2018.10.007, 2019.
- Zhang, M., Tian, W., Chen, L., and Lü, D.: Cross-tropopause mass exchange associated with a tropopause
- 716 fold event over the northeastern Tibetan Plateau. Advances in Atmospheric Sciences 27, 1344–1360.
- 717 https://doi.org/10.1007/s00376-010-9129-9, 2010.
- 718 Zhang, Y., Li, J., Yang, W., Du, H., Tang, X., Ye, Q., Wang, Z., Sun, Y., Pan, X., Zhu, L., and Wang, Z.:
- 719 Influences of stratospheric intrusions to high summer surface ozone over a heavily industrialized region
- 720 in northern China. Environmental Research Letters, 17, 094023. https://doi.org/10.1088/1748-
- 721 <u>9326/ac8b24</u>, 2022.

- 722 Zhao, K., Huang, J., Wu, Y., Yuan, Z., Wang, Yongwei, Li, Y., Ma, X., Liu, X., Ma, W., Wang, Ying, and
- 723 Zhang, X.: Impact of Stratospheric Intrusions on Ozone Enhancement in the Lower Troposphere and
- 724 Implication to Air Quality in Hong Kong and Other South China Regions. Journal of Geophysical
- 725 Research: Atmospheres, 126, e2020JD033955. https://doi.org/10.1029/2020JD033955, 2021.